Monthly Notices of the ROYAL ASTRONOMICAL SOCIETY

MNRAS **452,** 146–157 (2015) doi:10.1093/mnras/stv1244

Dynamical masses of a nova-like variable on the edge of the period gap

P. Rodríguez-Gil,[1,2,3★] T. Shahbaz,[1,2] T. R. Marsh,[4] B. T. Gänsicke,[4] D. Steeghs,[4] K. S. Long,[5] I. G. Martínez-Pais,[1,2] M. Armas Padilla,[1,2†] R. Schwarz,[6] M. R. Schreiber,[7] M. A. P. Torres,[8] D. Koester,[9] V. S. Dhillon,[10] J. Castellano[11] and D. Rodríguez[12]

[1]*Instituto de Astrofísica de Canarias, Vía Láctea s/n, La Laguna, E-38205 Tenerife, Spain*
[2]*Departamento de Astrofísica, Universidad de La Laguna, La Laguna, E-38206 Tenerife, Spain*
[3]*Harvard–Smithsonian Center for Astrophysics, 60 Garden St, Cambridge, MA 02138, USA*
[4]*Department of Physics, University of Warwick, Coventry CV4 7AL, UK*
[5]*Space Telescope Science Institute, 3700 San Martin Drive, Baltimore, MD 21218, USA*
[6]*Leibniz-Institut für Astrophysik Potsdam (AIP), An der Sternwarte 16, D-14482 Potsdam, Germany*
[7]*Departamento de Física y Astronomía, Universidad de Valparaíso, Avenida Gran Bretaña 1111, 2360102 Valparaíso, Chile*
[8]*SRON, Netherlands Institute for Space Research, Sorbonnelaan 2, NL-3584 CA Utrecht, the Netherlands*
[9]*Institut für Theoretische Physik und Astrophysik, University of Kiel, D-24098 Kiel, Germany*
[10]*Department of Physics and Astronomy, University of Sheffield, Sheffield S3 7RH, UK*
[11]*Observatorio Rodeno (MPC 939), Segorbe, E-12400 Castellón, Spain*
[12]*Observatorio Guadarrama (MPC 458), E-28430 Madrid, Spain*

Accepted 2015 June 1. Received 2015 May 27; in original form 2015 April 13

ABSTRACT

We present the first dynamical determination of the binary parameters of an eclipsing SW Sextantis star in the 3–4 h orbital period range during a low state. We obtained time-resolved optical spectroscopy and photometry of HS 0220+0603 during its 2004–2005 low-brightness state, as revealed in the combined Small & Moderate Aperture Research Telescope System, IAC80 and M1 Group long-term optical light curve. The optical spectra taken during primary eclipse reveal a secondary star spectral type of M5.5 ± 0.5 as derived from molecular band-head indices. The spectra also provide the first detection of a DAB white dwarf in a cataclysmic variable. By modelling its optical spectrum we estimate a white dwarf temperature of 30 000 ± 5000 K. By combining the results of modelling the white dwarf eclipse from ULTRACAM light curves with those obtained by simultaneously fitting the emission- and absorption-line radial velocity curves and *I*-band ellipsoidal light curves, we measure the stellar masses to be $M_1 = 0.87 \pm 0.09$ M$_\odot$ and $M_2 = 0.47 \pm 0.05$ M$_\odot$ for the white dwarf and the M dwarf, respectively, and an inclination of the orbital plane of $i \approx 79^\circ$. A radius of 0.0103 ± 0.0007 R$_\odot$ is obtained for the white dwarf. The secondary star in HS 0220+0603 is likely too cool and undersized for its mass.

Key words: binaries: close – stars: fundamental parameters – stars: individual: HS 0220+0603 – novae, cataclysmic variables.

1 INTRODUCTION

Cataclysmic variables (CVs) are binary systems that contain late-type (K–M) companion stars that fill their Roche lobes and therefore transfer mass to their white dwarf (WD) primary stars. Nova-like (NL) variables are CVs for which a nova or dwarf nova outburst has never been observed. The orbital period distribution of CVs shows a significant paucity of systems in the ∼2–3 h range, the so-called period gap (see e.g. Gänsicke et al. 2009, and references therein). CVs with orbital periods above the period gap are expected to have M-dwarf secondary stars up to a period of about ∼5.8 h, while secondary stars of earlier type are to be found for longer orbital periods (Knigge 2006). It is also just above the period gap, between 3 and 4 h, where a large population of CVs with extreme behaviour is found (Thorstensen et al. 1991; Rodríguez-Gil et al. 2007). There is mounting evidence that the NLs that populate this orbital period interval harbour intrinsically very bright accretion discs and very hot WDs (Townsley & Bildsten 2003; Araujo-Betancor et al. 2005; Townsley & Gänsicke 2009) that current evolutionary theories are unable to account for. In addition, at least 50 per cent of them belong to the SW Sextantis class (Rodríguez-Gil et al. 2007). Their large intrinsic accretion luminosities completely outshine both the WD

★ E-mail: prguez@iac.es, prodrigu@ull.es
† CEI Canarias: Campus Atlántico tricontinental.

© 2015 The Authors
Published by Oxford University Press on behalf of the Royal Astronomical Society

Downloaded from https://academic.oup.com/mnras/article-abstract/452/1/146/1748480/Dynamical-masses-of-a-nova-like-variable-on-the
by University of Sheffield user
on 17 October 2017

and its companion most of the time, making direct observations and accurate binary parameter measurements impossible (Ciardi et al. 1998). However, these CVs are occasionally caught fading towards states of greatly diminished brightness, or 'low states'. During the low states, these CVs are 3–5 mag fainter than their normal high state. They can stay at this level for days, months or even years before returning to the high state. Low states appear to be a feature of several types of CV and, in addition, they seem to occur independently of the magnetic field of the WD: they are observed in practically all known strongly magnetic systems without discs (polars), some intermediate polars and many weakly-magnetic CVs, including a large fraction of NLs and a number of dwarf novae (e.g. Schreiber, Gänsicke & Mattei 2002; Manser & Gänsicke 2014).

Although there is broad agreement that low states are the consequence of a reduction in the mass transfer rate from the donor star, the exact mechanism is unclear. Livio & Pringle (1994) and King & Cannizzo (1998) proposed an accumulation of large starspots close to the inner Lagrangian point (L1) as a way of inhibiting Roche lobe overflow, but Howell et al. (2000) put the case of the polar ST LMi forward to challenge this scenario and proposed that it is changes in the level of magnetic activity of the secondary star that may be behind the observed high-/low-state transitions. This idea had been already explored by Bianchini (1992), who invoked solar-like magnetic cycles with time-scales of about a decade.

In the low state, only gas provided by the magnetic activity or stellar wind of the donor star would then be available for accretion (e.g. Hessman, Gänsicke & Mattei 2000). In this respect, entanglement of the magnetic fields of both stars has been proposed to explain the line emission patterns observed in polars during low states (e.g. Kafka et al. 2008; Mason et al. 2008).

The study of the CV population with orbital periods between 3 and 4 h is of essential interest to the development of the theory of CV evolution. Particularly, those NL systems closer to the upper boundary of the period gap at an orbital period of about 3.18 h (a limit set observationally by Knigge 2006). According to the standard stellar structure codes (e.g. Chabrier & Baraffe 1997), the M-dwarf secondary stars in these CVs are expected to undergo a major change in their internal structure, developing into a totally convective configuration at a mass of $\sim$0.35 $M_\odot$. The exact value of this boundary depends on the choice of several parameters, such as the metallicity, opacities and mixing length (e.g. Chabrier & Baraffe 1997). We can find in the literature values ranging from 0.27 (Gabriel 1969) to 0.4 $M_\odot$ (Cox & Giuli 1969). For low-mass stars, Reiners & Mohanty (2012) place 0.3 $M_\odot$ as the fully convective limit. In the case of detached white dwarf/main-sequence binaries a drop in the fraction of post-common envelope binaries relative to wide binaries is observed at a mass of $\gtrsim$0.25 $M_\odot$, which is an independent observation in support of the disrupted magnetic braking mechanism invoked to reproduce the observed orbital period gap in CVs (Schreiber et al. 2010). On the other hand, in the population synthesis study of CVs by Howell, Nelson & Rappaport (2001) their zero-age main-sequence models have a fully convective configuration at a mass of $\sim$0.34 $M_\odot$, while the semi-empirical donor star sequence for CVs of Knigge (2006) suggests a (fully convective) donor mass of 0.2 $M_\odot$ at the upper edge of the period gap. These authors warn against the lack of fundamental input in the form of accurate masses, especially in the 3–4 h orbital period range. In fact, the donor masses used in this period interval come from *indirect* methods such as the mass ratio (q)–superhump period excess (ε) relation refined by Patterson et al. (2005), and the a priori assumption of a constant WD mass of 0.75 $M_\odot$. Moreover, the system used to refine the fit to the q–ε data, thought to have the largest value of the superhump excess ($\varepsilon = 0.094$), is BB Doradus, (Rodríguez-Gil et al. 2012; Schmidtobreick et al. 2012) for which an accurate determination of its stellar masses is unavailable.

Another essential observational input to the theory is the time-averaged mass transfer rate, that has to be compared with the predicted secular mass transfer rates (see Knigge, Baraffe & Patterson 2011). A medium-term (10^3–10^5 yr) mass transfer rate may be derived from measurements of the effective temperature and mass of the accreting WD (Townsley & Bildsten 2003; Townsley & Gänsicke 2009), which again emphasizes the need for accurate binary parameters.

In brief, no direct measurement of the stellar masses in any SW Sex star in the 3–4 h orbital period range exists thus far. However, the CV evolution theory demands appropriate input in the form of dynamical mass solutions and other binary parameters. This is especially true for these CVs close to the upper boundary of the period gap, in which the donor stars may be about to experience the predicted major structural change in their stellar interiors.

In this paper, we present the first attempt to measure the fundamental parameters of an SW Sex star in the 3–4 h period range, the eclipsing system HS 0220+0603 (Rodríguez-Gil et al. 2007), with no initial assumptions about the binary system.

2 LONG-TERM LIGHT CURVE

The long-term V-band light curve of HS 0220+0603 is presented in Fig. 1. The photometry spans 9.92 years and comprises data provided by Spanish amateur astronomers of the M1 Group, the

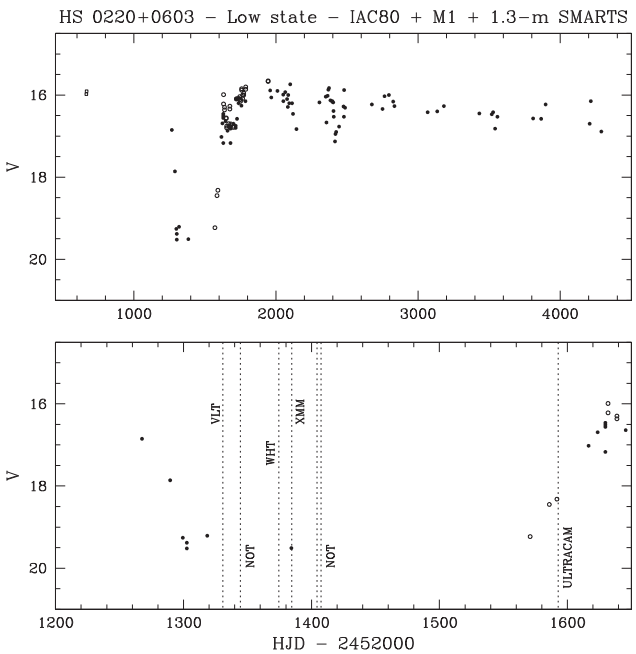

Figure 1. Top panel: long-term, V-band light curve of HS 0220+0603 showing 9.92 years of photometry from 2003 Jan 26 to 2012 Dec 26. Data from the Spanish amateur astronomers of the M1 Group (filled circles), the 1.3-m SMARTS telescope on Cerro Tololo (open circles) and the 0.82-m IAC80 telescope on Tenerife (open squares; first two data points) are shown. Data taken during eclipse are also included in the plot. Bottom panel: zoomed version of the top panel showing the low state data only. The vertical dashed lines mark the dates of the spectroscopic, photometric and XMM UV observations detailed in Section 3.

Downloaded from https://academic.oup.com/mnras/article-abstract/452/1/146/1748480/Dynamical-masses-of-a-nova-like-variable-on-the
by University of Sheffield user
on 17 October 2017

1.3-m SMARTS telescope on Cerro Tololo, Chile (operated by the SMARTS Consortium) and the 0.82-m IAC80 telescope at the Observatorio del Teide on Tenerife, Spain. The apparent V-band magnitudes were computed relative to the comparison star USNO–A2.0 0900–00554112. Conversion of its $B_{A2.0}$ and $R_{A2.0}$ magnitudes into the Landolt standard system[1] resulted in a V-band magnitude of 12.3. The nearby star USNO–A2.0 0900–00553941 ($V = 16.5$) was used as the check star.

The M1 Group reported HS 0220+0603 entering a low state on 2004 September 19. The system was at $V = 16.8$, nearly a magnitude fainter than the previous IAC80 telescope measurements. Almost a month later, on 2004 October 24, the system settled in the low state at $V = 19.5$ after fading at a rate of $\sim$0.08 mag d^{-1}. The egress from the low state occurred shortly before 2005 July 19, when the system was observed at $V = 19.2$. It then brightened at a relatively slow rate of $\sim-$ 0.05 mag d^{-1} and reached its high state brightness level at $V \approx 16$ around 2005 September 18. This places a lower limit to the low state length of about 1 year. However, just after 2005 September 18 it started to fade again at a rate of $\sim$0.03 mag d^{-1}. HS 0220+0603 remained at $V \approx 16.7$ for about 64 d before starting its final rise to the high state at the same rate of $\sim-$ 0.03 mag d^{-1}. All the ingress and egress slopes reported here have to be taken with caution due to the scarce sampling of the long-term light curve, but the occurrence of the second fading looks convincing. Further, during this secondary plateau the system showed occasional brightenings with an amplitude of $\sim$0.5 mag, similar to those seen in BB Dor in the low state (Rodríguez-Gil et al. 2012). Finally, the post-low-state monitoring reveals a steady brightness decline at a rate of $\sim 3 \times 10^{-4}$ mag d^{-1}.

3 DATA ACQUISITION AND REDUCTION

3.1 Optical spectroscopy

3.1.1 Very Large Telescope

We obtained four 600-s spectra with the ESO 8.2-m Very Large Telescope (VLT) at Cerro Paranal on 2004 November 20, shortly after the onset of minimum light with the FOcal Reducer and low dispersion Spectrograph on the Antu (UT1) telescope. For the observations the spectrograph was equipped with the 600RI grism, the GG435 order sorter filter and the MIT/LL 2048 × 4096 pixel CCD detector. With a 0.7-arcsec slit, this delivered a spectral resolution of 3.5 Å (full width at half-maximum, FWHM) over the 5015–8325 Å wavelength range. For flux calibration we used spectra of the flux standard LTT 377.

3.1.2 William Herschel Telescope

We carried out time-resolved spectroscopy of HS 0220+0603 on 2005 January 3 with the 4.2-m William Herschel Telescope (WHT) at the Roque de los Muchachos Observatory on La Palma. The double-armed Intermediate dispersion Spectrograph and Imaging System (ISIS) was fitted with the R600B and the R316R gratings, and the 2048 × 4200 pixel EEV12 and the 2148 × 4700 pixel Marconi CCDs in the blue and the red arm, respectively. This setup and a 1.2-arcsec slit width ($\simeq$1.5-arcsec seeing conditions) granted access to the wavelength intervals 3700–5010 and 6110–8930 Å at 1.8 and 3.3 Å resolution (FWHM) in the blue and red, respectively.

[1] See http://www.pas.rochester.edu/~emamajek/memo_USNO-A2.0.html.

Table 1. Log of optical observations.

UT date	Coverage (h)	Filter/Grating	Exp. (s)	No. of Frames
VLT, FORS2 spectroscopy				
2004 Nov 20	0.54	GRIS_600RI	600	4
WHT, ISIS spectroscopy				
2005 Jan 03	3.92	R600B/R316R	1200/1200	12/12
NOT, ALFOSC photometry				
2004 Dec 04	3.62	I#11	40, 60	181
2005 Feb 02	2.22	I#11	30, 40, 60	107
2005 Feb 05	2.35	I#11	40, 80	142
WHT, ULTRACAM photometry				
2005 Aug 09	4.27	u', g', i'	4.95	3089
2005 Aug 10	3.93	u', g', i'	4.95	2841

The exposure time was 1200 s and we regularly took spectra of arc lamps in order to account for instrument flexure. A flat-field image was obtained after every two science exposures of the target in order to correct for fringing in the red-arm CCD. Flux calibration was performed using spectra of the flux standard Feige 34 taken with the same setup. We used the same spectrophotometric standard star to remove the telluric features. See Table 1 for details of the observations.

We reduced both the VLT and WHT spectroscopic data using standard procedures in IRAF.[2] After subtracting the bias level, the images were divided by an average flat-field that was normalized by fitting Chebyshev functions of high order to remove the detector specific spectral response. We then subtracted the sky contribution and optimally extracted the final spectra following the method described by Horne (1986). For wavelength calibration, we fitted a low-order polynomial to the pixel-wavelength arc data. In calibrating the WHT data, we obtained the wavelength solution for each target spectrum by interpolating between the two nearest arc spectra. All subsequent analysis was performed with the MOLLY[3] package. All the spectra were corrected for interstellar reddening using a colour excess of $E(B - V) = 0.047$, corresponding to $A_V = 0.145$ mag (from the extinction map of Schlafly & Finkbeiner 2011).

3.2 Optical photometry

3.2.1 NOT I-band light curves

We used the Andalucía Faint Object Spectrograph and Camera (ALFOSC) equipped with the 2048 × 2048 pixel EEV chip (CCD #8) on the 2.56-m Nordic Optical Telescope (NOT) on La Palma to obtain time-resolved, I-band photometry of HS 0220+0603 on 2004 December 4 and 2005 February 2 and 5. The exposure time ranged between 30 and 80 s due to changing sky transparency conditions during the nights. We used IRAF to reduce the individual images in a standard way, and to perform aperture photometry on the target and two comparison stars. Differential light curves of the target relative to the main comparison star (C_1, USNO–A2.0 0900–00554015) were then computed. We confirmed the stability of C_1 by differential photometry relative to the second comparison star. In converting the differential I-band magnitudes of HS 0220+0603

[2] IRAF is distributed by the National Optical Astronomy Observatories.
[3] http://deneb.astro.warwick.ac.uk/phsaap/software/molly/html/INDEX.html

Downloaded from https://academic.oup.com/mnras/article-abstract/452/1/146/1748480/Dynamical-masses-of-a-nova-like-variable-on-the
by University of Sheffield user
on 17 October 2017

to the standard system, we calculated the *I*-band magnitude of C_1 from its Sloan Digital Sky Survey (SDSS) *r*, *i* and *z* magnitude measurements (Data Release 7). We then transformed the SDSS magnitudes into *I*-band magnitudes by using the two formulae given by R. Lupton in 2005.[4] The average value for C_1 is $I = 15.565 \pm 0.007$.

3.2.2 *WHT/ULTRACAM fast photometry*

We also observed HS 0220+0603 with ULTRACAM on the WHT on La Palma on 2005 August 9 and 10. ULTRACAM is a high-speed, triple-beam CCD camera (Dhillon et al. 2007) capable of acquiring simultaneous images in three different photometric bands. For HS 0220+0603, we used the SDSS u', g' and i' filters (see Table 1). The exposure time was fixed to 4.95 s and the dead time between consecutive exposures was ∼24 ms. We reduced the data with the ULTRACAM pipeline software. Debiasing, flat-fielding and sky subtraction were performed in the standard way. We determined the flux of the source and two close comparison stars with aperture photometry using a variable aperture scaled according to the FWHM of the stellar profile. Note that the ULTRACAM observations took place when the system's brightness was starting to increase (see Fig. 1), and it was about one magnitude brighter than the low state level.

3.2.3 *Updated eclipse ephemeris*

We combined the times of mid-eclipse of the WD in HS 0220+0603 in the high state reported by Rodríguez-Gil et al. (2007) with new WD mid-eclipse times measured from the light curves in the low state presented in this work to update the eclipse ephemeris. The resulting linear ephemeris is

$$T_0(\mathrm{HJD}) = 2452563.57399(12) + 0.149207749(75) \times E \ .$$

We used this ephemeris to calculate the orbital phase for all the data presented in this work.

4 *XMM–NEWTON* X-RAY AND UV OBSERVATIONS

The *XMM–Newton* satellite (Jansen et al. 2001) pointed to HS 0220+0603 for 30.7 ks on 2015 January 13 (observation ID 0212480101). The European Photon Imaging Camera consists of two MOS cameras (Turner et al. 2001) and one PN camera (Strüder et al. 2001), which were operated in full-frame window imaging mode with the thin optical blocking filter applied. We used the Science Analysis Software (SAS, v.14.0) to carry out the data reduction and obtain the scientific products. The observation was affected by episodes of background flaring, therefore a total of 14.2 ks had to be neglected in our analysis. We extracted events using a circular region with a radius of 15 arcsec centred on the source position (RA = 02:23:01.6, Dec. = +06:16:49.6, J2000), and a circular region with a radius of 30 arcsec covering a source-free part of the CCDs to extract background events. The average 0.2–12 keV source net count rate was $(8.2 \pm 1.0) \times 10^{-3}$ count s^{-1} for the PN camera. A very limited number of photons were recorded with the MOS cameras, which did not allow us to perform a spectral analysis.

We generated the spectrum and the light curve of the PN data, as well as the response files, following the standard analysis threads.[5]

[4] http://www.sdss3.org/dr8/algorithms/sdssUBVRITransform.php
[5] http://www.pas.rochester.edu/~emamajek/memo_USNO-A2.0.html

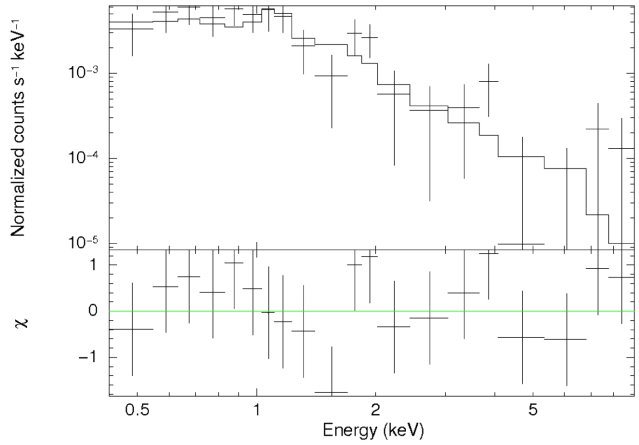

Figure 2. The 0.3–10 keV PN X-ray spectrum (top) and residuals (bottom). The solid line represents the best fit with a one-temperature thermal plasma model (PHABS*APEC).

Table 2. Best fit to the 0.3–10 keV PN spectrum using PHABS*APEC.

Model parameters			
N_H	3.2×10^{20} cm^{-2}		
kT	2.9 keV		
EM[a, b]	8.98×10^{52} cm^{-3}		
χ^2 (dof)	0.7 (18)		
Energy band	$F_{X,abs}$ (10^{-14} erg cm^{-2} s^{-1})	$F_{X,unabs}$	L_X[b] (10^{29} erg s^{-1})
0.5–10 keV	2.0	2.1	14
0.1–7 keV	2.03	2.4	16
0.5–10 keV	1.25	1.62	10

[a]Emission measure EM= $\int n_e n_H dV = 4\pi D^2 \mathrm{Norm}_{\mathrm{APEC}}$.
[b]To calculate the EM and the luminosities $D = 740$ pc was assumed for the distance.

The spectral data were grouped to contain a minimum of 10 photons per bin and fit in the 0.3–10 keV energy range using XSPEC (v.12.8; Arnaud 1996). We assumed a total Galactic H I column density (N_H) of N_H=$(3.2 \pm 0.1) \times 10^{20}$ cm^{-2} calculated with the N_H–A_V relation (Güver & Özel 2009) using the A_V obtained in Section 3.1. This is consistent with the N_H=4.8×10^{20} cm^{-2} in the direction to the source found by Kalberla et al. (2005).

Since HS 0220+0603 is in a low state, we assume that the bulk of the X-ray emission comes from the M-dwarf companion star. Therefore, we modelled the spectrum with an absorbed one-temperature thermal plasma model, which is typically used for stellar emission. To this end, the plasma thermal emission APEC code (Smith et al. 2001) was applied. A good fit with χ^2_ν=0.7 for 18 degrees of freedom (dof) and *p*-value >0.8 (see Fig. 2) was achieved. The value of the obtained temperature is $kT = 2.9$ keV (∼34 MK) and the emission measure (EM) is 8.98×10^{52} cm^{-3}. The 0.5–10 keV absorbed (unabsorbed) flux is 2.0×10^{-14} erg cm^{-2} s^{-1} (2.1×10^{-14} erg cm^{-2} s^{-1}). Assuming a distance of 740 pc (see Section 6.2), the corresponding X-ray luminosity is 14×10^{29} erg s^{-1} (see Table 2 for spectral results and X-ray luminosities for different energy ranges in order to compare with the literature).

Our results are comparable with those obtained for single M-dwarf stars (Schmitt & Liefke 2004), although in our case the luminosity is higher (approximately one order of magnitude). For example, LMC 335 and 2XMM J043527.2–144301 have

Downloaded from https://academic.oup.com/mnras/article-abstract/452/1/146/1748480/Dynamical-masses-of-a-nova-like-variable-on-the
by University of Sheffield user
on 17 October 2017

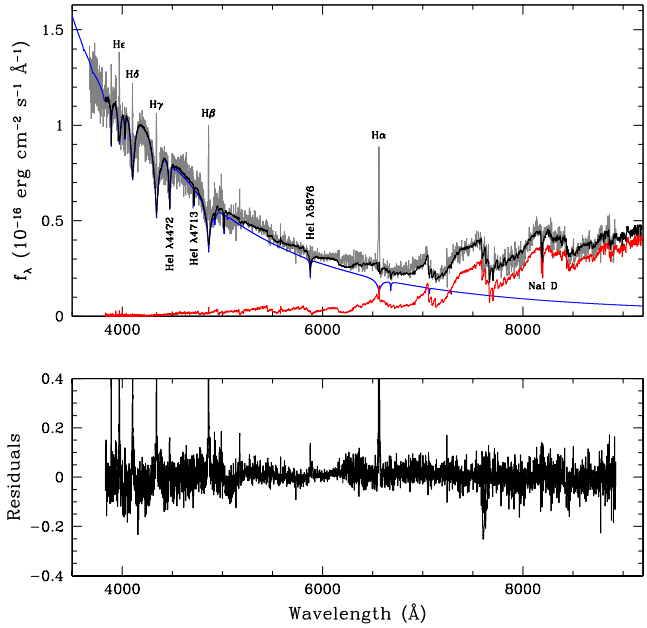

Figure 3. Average VLT/FORS and WHT/ISIS spectrum of HS 0220+0603. Only spectra taken shortly before or after primary eclipse were used in order to include the WD spectrum while at the same time minimizing the effect of irradiation from the WD on the M-dwarf companion. The data (grey) are fitted with WD (blue)+M-dwarf (red) templates. The solid black line is the best composite fit (see text for details).

temperatures of $kT = 1.22$ keV and $kT = 1.7$ keV, and X-ray luminosities of 1.7×10^{29} erg s^{-1} (0.1–7 keV) and 5×10^{27} erg s^{-1} (0.2–2 keV), respectively (Gupta, Galeazzi & Williams 2011; Tsang et al. 2012). When placing HS 0220+0603 in the L_X versus rotation period plot (Pizzolato et al. 2003, see also Cook, Williams & Berger 2014), we see that the luminosity is also higher than rapidly rotating active stars. We therefore cannot discard the presence of X-ray emission due to very low-level accretion.

Simultaneous to the X-ray measurements, observations with the optical/UV monitor telescope (Mason et al. 2001) were carried out in the imaging mode. The near-ultraviolet *uvw*1 (245–320 nm) and *uvm*2 (205–245 nm) filters were used during ∼4.4 ks each. The data were reduced using the `omichain` task. The resulting unreddened fluxes for the *uvw*1 and *uvm*2 bands were $(0.24 \pm 0.01) \times 10^{-15}$ erg cm^{-2} s^{-1} Å^{-1} and $(0.48 \pm 0.02) \times 10^{-15}$ erg cm^{-2} s^{-1} Å^{-1}, respectively (see the bottom panel of Fig. 4).

5 SPECTRAL CLASSIFICATION

5.1 Spectral energy distribution

The optical spectrum of HS 0220+0603 in the low state is dominated by the two stellar components. In Fig. 3, the contributions of a WD and a mid-M dwarf are apparent in the blue and the red, respectively. The spectral modelling presented below does not require the presence of an accretion disc. In addition, the U-shaped WD eclipse seen in the light curves (see Figs 5 and 10) points to a bare WD or, at most, a WD surrounded by a cold, remnant disc. The emission lines do not reveal a disc either, unlike DW UMa in the low state (Dhillon, Jones & Marsh 1994).

Narrow emission lines of hydrogen are superimposed on the WD absorption troughs. For comparison, the intrinsic FWHM of Hα in the low state is 340 km s^{-1} at orbital phase 0 (defined as inferior conjunction of the secondary star), whilst the Hα emission line has an FWHM of 1390 km s^{-1} in the high state (Rodríguez-Gil et al. 2007). The Ca II triplet (λ8498, λ8542 and λ8662) in emission is apparent around orbital phase 0.5. Some He I λ5876 emission is also present. We will later show that these narrow emission lines originate on the donor side of the binary system, and are due to irradiation from a hot WD and/or chromospheric emission. The He II λ4686 and Bowen blend emissions observed in the high state are absent.

In determining the spectral type of the two stars, we used an average spectrum of HS 0220+0603 computed from spectra corresponding to a limited range of orbital phases around the primary eclipse. This minimizes the contribution from the side of the secondary star that faces the WD and yet includes the spectrum of the WD. In particular, we only used VLT/FORS2 spectra obtained at orbital phases 0.15 and 0.20, WHT/ISIS red spectra at 0.92, 0.93 and 0.11, and at 0.82, 0.92, 0.93, 0.11 and 0.21 for the WHT/ISIS blue spectra. Note that we use this average spectrum in the subsequent analyses unless otherwise stated. Also note that this approach will eliminate any information on the spectral type variation with orbital phase, but it is necessary as the signal-to-noise ratio of the individual spectra is far from being optimal for this purpose.

The spectral contribution of the WD is very blue in colour, and contains both Balmer and He I lines, making this the first definite detection of a DAB WD in a CV. The composite spectrum superimposed on the average spectrum of HS 0220+0603 presented in Fig. 3 contains our DAB WD model with temperature and surface gravity of 30 000 K and $\log g = 8.35$, respectively, and a dwarf M5.5 secondary star (see Section 5.2).

The de-reddened UV fluxes (see Section 4) are plotted together with our WD model and the average WHT/ISIS blue spectrum in the bottom panel of Fig. 4. The UV observations fit well into the WD model with $T_{\rm eff} = 30\,000$ K. For comparison, we show in Fig. 4 the SDSS spectrum of a (single) DAB WD with similar atmospheric parameters (SDSS J084742.22+000647.6, $T_{\rm eff} = 30545 \pm 241$ K, $\log g = 8.49 \pm 0.05$; Kleinman et al. 2004) along with the average spectrum of the WD in HS 0220+0603 and the DAB model. The SDSS WD and the HS 0220+0603 spectra show a good match. Given the uncertainties in the flux calibration of the average WD spectrum and the UV fluxes, and considering that the UV and the optical observations were not simultaneous, it is difficult to establish a formal error on the WD temperature, but we conservatively estimate that the quoted value is accurate to within 5000 K.

5.2 Secondary star molecular-band indices

In this section, we present the determination of the spectral type of the secondary star. Boeshaar (1976) introduced a spectral classification scheme for M dwarfs based on molecular-band ratios, which has also been used for CVs (Wade & Horne 1988). The work of Reid, Hawley & Gizis (1995) used a similar set of spectral indices to measure the depth of selected molecular band heads. These authors improved on the M-dwarf spectral sequence presented by Kirkpatrick, Henry & McCarthy (1991) for classification in the red (6300–9000 Å). These indices have been extensively calibrated against spectral type by many authors (see Lépine, Rich & Shara 2003, and references therein).

An assessment of the spectral type of the secondary star in HS 0220+0603 can therefore be done by measuring a set of these

Downloaded from https://academic.oup.com/mnras/article-abstract/452/1/146/1748480/Dynamical-masses-of-a-nova-like-variable-on-the
by University of Sheffield user
on 17 October 2017

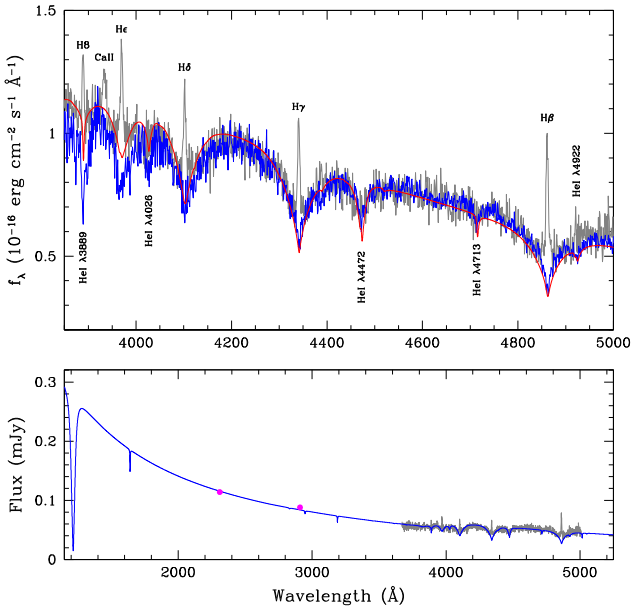

Figure 4. Top panel: average WD spectrum around eclipse (grey) with our DAB WD model (red; $T_{\rm eff} = 30\,000$ K, $\log g = 8.35$) and spectrum of the field DAB WD SDSS J084742.22+000647.6 (blue; $T_{\rm eff} = 30545$ K, $\log g = 8.49$) superimposed. Note that the contribution of the secondary star has not been subtracted, so there is a flux excess increasing with wavelength. Bottom panel: average WD spectrum around eclipse (grey) with our DAB WD model (blue) and the *XMM* UV flux measurements after correcting for interstellar reddening (circles).

spectral indices from the average WHT/ISIS red spectrum and comparing them with the indices observed for calibrated M dwarfs. We followed the strategy described by Lépine et al. (2003) for mid to late M-dwarfs, focusing on the VO1, VO2 and TiO7 indices (see their table 2 for details). We did not use the TiO6 index as the continuum is defined very close to the O_2 telluric absorption complex at ∼7650 Å, and residuals from the telluric correction remain in that region. Prior to this analysis, we first removed the contribution of the WD. We present the flux ratios for HS 0220+0603 and SDSS M-dwarfs ranging from M2 to M8 in Table 3. Lépine et al. (2003) present linear functions to obtain the spectral type of M dwarfs from the molecular-band indices. Using their equations (4), (6) and (7), we obtain a spectral type for the secondary star in HS 0220+0603 of M5.5, M5.6 and M5.4 for the VO1, VO2 and TiO7 indices, respectively. The indices obtained for the SDSS M-dwarf templates (Table 3) also point to an M5–6 spectral type. The linear calibrations of Lépine et al. (2003) can provide spectral types accurate to half a spectral type. We can therefore conclude that the M-dwarf

Table 3. Molecular band-head indices.

Star	VO1	VO2	TiO7
HS 0220+0603	0.875	0.649	0.756
M2V	0.947	0.899	0.956
M3V	0.920	0.821	0.914
M4V	0.904	0.758	0.876
M5V	0.874	0.654	0.791
M6V	0.851	0.601	0.762
M7V	0.829	0.537	0.703
M8V	0.799	0.443	0.626

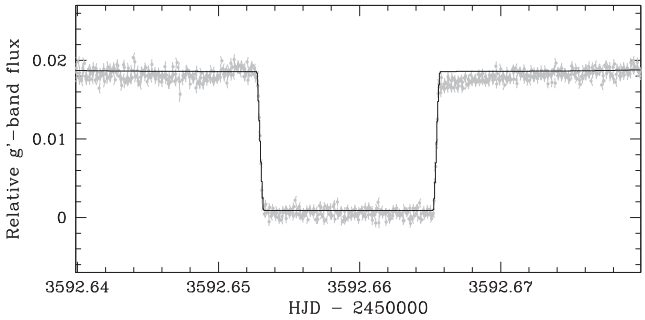

Figure 5. Modelling of the WHT/ULTRACAM WD eclipse in the g' band. The data were fitted with the LCURVE code. The solid line represents the best fit.

secondary star in HS 0220+0603 shows a low-state spectral type of M5.5 ± 0.5 when observed close to its inferior conjunction.

6 BINARY PARAMETERS

6.1 WD eclipse modelling

In order to obtain constraints on the binary parameters, we fitted light curve models to the ULTRACAM g'-band eclipse data. The g'-band light curve has the best quality and the deepest eclipse of the three recorded by ULTRACAM (see Fig. 5). Of special interest is the mass ratio $q = M_2/M_1$ (where M_1 and M_2 are the masses of the WD and secondary star, respectively) as a function of the orbital inclination (i), that can be tested against an analogous function derived from the joint modelling of the emission- and absorption-line radial velocity curves and the ellipsoidal modulation plus eclipse curves (see Section 6.2).

For the modelling of the ULTRACAM light curve, we made use of the LCURVE code developed by one of us (TRM; see Copperwheat et al. 2010 for a description, and e.g. Pyrzas et al. 2009 for its application to light curves of WD/M-dwarf binaries). The LCURVE code computes a model from input parameters provided by the user. Model light curves are then fitted to the data using Levenberg–Marquardt minimization. Both fixed and free parameters can be set by the user, which gives full flexibility to the code operation.

The results of the spectral modelling presented in Section 5.1 allowed us to fix the temperature of the WD to $T_1 = 30\,000$ K. We also fixed the limb darkening coefficients to four-parameter values as listed in Gianninas et al. (2013) for $T_1 = 30\,000$ K and $\log g = 8.5$. The mass ratio q, the scaled WD radius $r_1 = R_1/a$ (with a the binary separation) and the effective temperature of the secondary star T_2 were left as free parameters. For the scaled secondary star radius $r_2 = R_2/a$, the code calculates the proper non-spherical shape of the secondary star's Roche lobe for each value of q. We performed a grid search in q, with q ranging from 0.25 to 0.60 in steps of 0.05. The results are presented in Table 4.

6.2 Simultaneous radial velocity and ellipsoidal modulation modelling

The NOT I-band light curves were phase folded according to the eclipse ephemeris given in Section 3.2.3 and averaged into 43 orbital phase bins. To interpret the I-band light curve and the absorption- and emission-line radial velocity curves we used the XRBCURVE model described in Shahbaz et al. (2003), which has successfully been used to model the light curves and radial velocity curves of neutron star and black hole X-ray binaries (Shahbaz et al. 2004).

Downloaded from https://academic.oup.com/mnras/article-abstract/452/1/146/1748480/Dynamical-masses-of-a-nova-like-variable-on-the
by University of Sheffield user
on 17 October 2017

Table 4. ULTRACAM WD eclipse modelling parameters.

Mass ratio $q(=M_2/M_1)$	Inclination i (deg)	Scaled WD radius $r_1(=R_1/a)$
0.260	88.71(15)	0.0101(5)
0.300	85.48(04)	0.0095(5)
0.350	83.51(03)	0.0091(4)
0.400	82.11(03)	0.0087(5)
0.450	80.99(02)	0.0083(4)
0.500	80.05(02)	0.0080(4)
0.550	79.24(02)	0.0078(4)
0.600	78.52(02)	0.0075(4)

Briefly, the model includes a Roche lobe filling secondary star, the effects of UV/X-ray heating of the secondary star by a source of high-energy photons from a compact object, an accretion disc and mutual eclipses of the disc and star. In the case of HS 0220+0603 in the low state, where the eclipse of the WD by the secondary star is clearly seen, we simulate the presence of a bare WD by assuming that it can be described by a blackbody cylindrical accretion disc (with equal radius and height).

The geometry of the binary system is given by the orbital inclination i, the binary mass ratio q, and the Roche lobe filling factor f_{R_2} of the secondary star. The light arising from the secondary star depends on its mean effective temperature (T_2), the gravity darkening exponent β and the X-ray/UV albedo W. The additional light due to UV/X-ray heating is given by the unabsorbed UV/X-ray flux ($F_{X,0}$). The light from the WD is given by its scaled radius and effective temperature. The distance to the source in parsecs (d_{pc}), the orbital period P and the radial velocity amplitude of the secondary star (K_2) set the scale of the system.

We use PHOENIX model-atmosphere fluxes (Hauschildt, Allard & Baron 1999) to determine the intensity distribution on the secondary star and blackbody fluxes for the light arising from the WD. For both cases we use a quadratic limb-darkening law with coefficients taken from Claret (1998), to correct the intensity. We assume that the secondary star is in synchronous rotation and completely fills its Roche lobe. Since the late-type secondary star should have a convective envelope, we fix the gravity darkening exponent to 0.08 (Lucy 1967). Its albedo (W) is fixed at 0.40 (de Jong, van Paradijs & Augusteijn 1996).

The irradiating flux can strongly alter the distribution of temperature across the face of the secondary star and thus the observed optical light curves and radial velocities. For the light curves, the heating of the secondary star is computed in the same way as described in Shahbaz et al. (2003), who calculate the increase in unperturbed local effective temperature due to the irradiating external source. Substantial heating of the secondary star also shifts the effective centre of the secondary, weighted by the strength of the absorption and emission lines, from the centre of mass of the star. This results in a significant distortion of the radial velocity curve leading to spuriously high or low K-amplitudes using absorption or emission lines, respectively, arising from the secondary star (Phillips, Shahbaz & Podsiadlowski 1999; Shahbaz et al. 2000). To model the radial velocity curves, we determine the fraction of the surface of the star that contributes to the absorption-line or emission-line radial velocity. These are described by factors F_{AV} and F_{EV}, respectively, and represent the fraction of the external radiation flux that exceeds the unperturbed flux, e.g. F_{AV}=1.0 assumes all the area of the star visible by the heating source is irradiated and does not contribute to the absorption-line radial velocity, whereas for F_{EV}=1.10 only surface elements on the star where the external radiation flux is greater than 10 per cent of the unperturbed flux contribute to the emission-line radial velocity (Billington, Marsh & Dhillon 1996; Phillips et al. 1999). The line flux of each element on the star is calculated using the equivalent width and continuum flux value, and the equivalent width of elements that do not contribute are set to zero. For ease of reference, the key variables are listed in Table 5.

Table 5. List of the key model variables and what they represent.

Variable	Definition
M_1	Mass of the WD
M_2	Mass of the secondary star
q	Binary mass ratio defined as M_2/M_1
i	Orbital inclination
P	Orbital period
a	Binary separation
$F_{X,0}$	Unabsorbed heating flux
d_{pc}	Distance in pc
K_2	Secondary star's radial velocity amplitude
T_2	Secondary star's mean effective temperature
R_1	WD radius
T_1	WD effective temperature
β	Gravity darkening exponent
W	Albedo of the secondary star
$E(B-V)$	Colour excess

In determining the binary parameters we simultaneously fit the photometric I-band light curve (43 data points) and the absorption-line (Na I doublet) and emission-line (Ca II triplet) radial velocity curves (11 and 7 data points, respectively) with our model to represent the photometric and radial velocity variations. We used the differential evolution algorithm described in Shahbaz et al. (2003) to fit the data, which is robust and simple.

The model parameters that determine the shape and amplitude of the optical light curves, absorption-line and emission-line radial velocity curves are i, q, T_2, $F_{X,0}$, d_{pc}, W, R_1, T_1, K_2, F_{AV} and F_{EV}. For the fitting procedure, there are three extra parameters: the phase shift for the optical light curve $\delta\phi_{LC}$, and the phase and radial-velocity shift for the absorption-line radial velocity curve $\delta\phi_{RV}$ and γ_{RV}, respectively (the absorption-line radial velocity curve allows us to define the phase 0.0, i.e. inferior conjunction of the secondary star, and the systemic velocity, hence we use the same values for the fit to the emission-line radial velocity curve).

We fixed $T_2 = 3000$ K for a mid-M dwarf (see e.g. Leggett et al. 1996), a WD blackbody temperature of $T_1 = 30\,000$ K, $E(B-V) = 0.047$ with the constraint $M_1 < 1.4$ M$_\odot$ and then performed a grid search in i. Given that there are three different data sets with different numbers of data points, to optimize the fitting procedure we assigned relative weights to them. After our initial search of the parameter space, which resulted in a good solution, we scaled the uncertainties on each data set (i.e. the light curve and the radial velocity curves) so that the total reduced χ^2 of the fit was ∼1 for each data set separately. The fitting procedure was then repeated to produce the final set of parameters. We have checked that the results do not significantly change upon varying T_2 by a few hundred degrees.

By combining the best-fitting model parameters q, i and K_2 with the mass function equation, we can determine M_1 and M_2. In Fig. 6, we show the best-fitting solutions in the (M_1–M_2) plane, where the most probable value for the binary masses are $M_1 = 0.87$ M$_\odot$ and $M_2 = 0.47$ M$_\odot$. The red circles in the figure show the 99 per cent confidence level solutions. Table 6 shows the mean and rms uncertainties in the parameters values, where we have only used

Downloaded from https://academic.oup.com/mnras/article-abstract/452/1/146/1748480/Dynamical-masses-of-a-nova-like-variable-on-the
by University of Sheffield user
on 17 October 2017

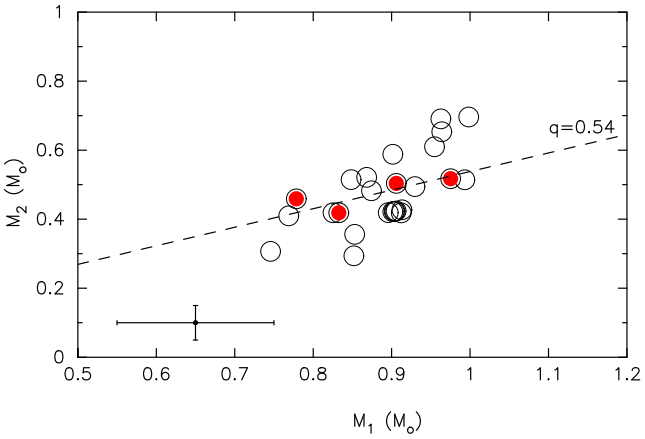

Figure 6. M_1–M_2 plane with the best-fitting solutions. The solid red circles show the 99 per cent confidence level solutions. The dashed line corresponds to a mass ratio of $q = 0.54$. The bars at the lower left represent the typical error.

solutions with the 99 per cent confidence level. As one can see the (M_1–M_2) solution allows us to constrain q; the dashed line in Fig. 6 shows the best fit with $q = 0.54 \pm 0.02$, which when combined with the ($i - q$) solutions obtained from the ULTRACAM eclipse fitting (see Section 6.1), gives $i \sim 79°$. In Fig. 7, we show the light curve and radial velocity curves for the best-fitting model parameters; $M_1 = 0.87\ \mathrm{M}_\odot$ and $M_2 = 0.47\ \mathrm{M}_\odot$, $i = 79°$, $T_2 = 3000$ K and $T_1 = 30\,000$ K.

We also present a model prediction of the H α emission-line radial velocity curve (not included in the fitting process) assuming that all of the inner face of the secondary star is irradiated. The model nicely

Table 6. Results obtained from the model fits to the *I*-band optical light curve, Na I absorption-line and Ca II emission-line radial velocity curves of HS 0220+0603 for $T_2 = 3000$ K and $T_1 = 30\,000$ K.

Parameter	Value
q	0.54 ± 0.03
K_2 (km s^{-1})	284 ± 11
d_{pc}	740 ± 26
log $F_{\mathrm{X,0}}$ (erg cm^{-2} s^{-1})	− 11.7 ± 0.05
γ_{AV} (km s^{-1})	1.8 ± 2.3
F_{AV}	1.06 ± 0.06
F_{EV}	1.03 ± 0.02
M_1 (M$_\odot$)	0.87 ± 0.09
M_2 (M$_\odot$)	0.47 ± 0.05

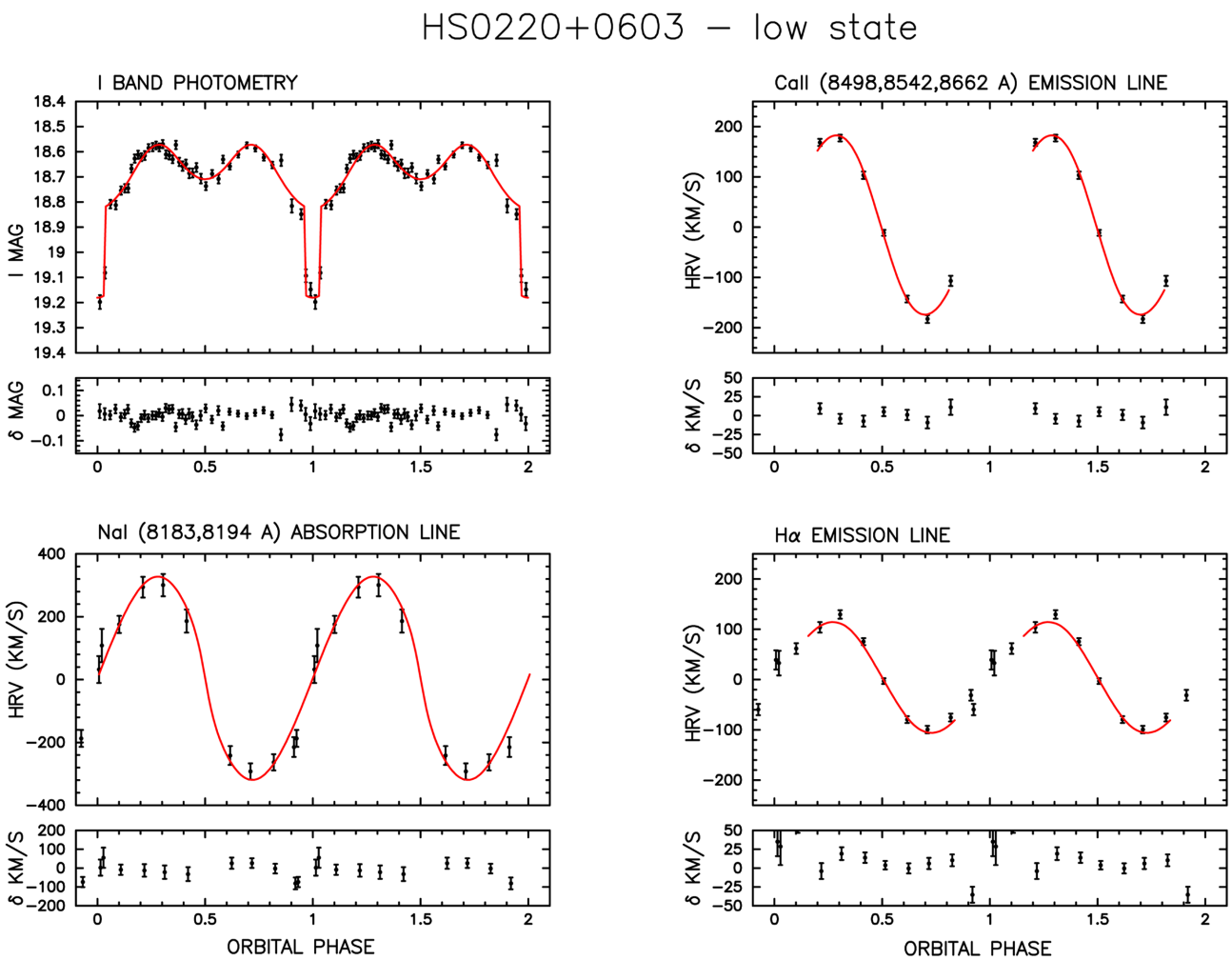

Figure 7. From left to right and from top to bottom: NOT *I*-band ellipsoidal+WD eclipse light curve; Ca II emission triplet heliocentric radial velocity (HRV) curve; Na I absorption doublet HRV curve; H α emission HRV curve. Solid lines are the best fits with the exception of H α (model-predicted curve). The plots under each panel are the corresponding residuals. The orbital cycle has been repeated for clarity.

Downloaded from https://academic.oup.com/mnras/article-abstract/452/1/146/1748480/Dynamical-masses-of-a-nova-like-variable-on-the
by University of Sheffield user
on 17 October 2017

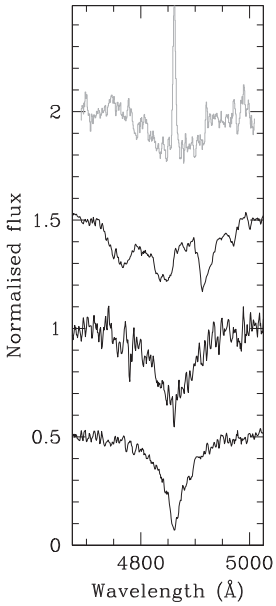

Figure 8. Comparison of the HS 0220+0603 average H β absorption profile (top grey spectrum) with the H β absorption profiles of three magnetic WDs (showing the characteristic Zeeman splitting) with magnetic fields of 8.4, 4.1 and 1.0 MG (from top to bottom; see text for details).

reproduces the observed H α radial velocity curve, but note that the H α emission line is also seen around zero phase, indicating that it is not entirely driven by irradiation. We suggest that chromospheric H α emission is also occurring in the secondary star (also see Mason et al. 2008, for the case of VV Pup in the low state).

7 DISCUSSION

7.1 The white dwarf

The spectral decomposition of the optical spectrum of HS 0220+0603 in the low state revealed a DAB WD with $T_{\rm eff} \simeq 30\,000$ K and $\log g \simeq 8.35$. On the other hand, our dynamical solution of the binary system provided a WD with mass $M_1 = 0.87 \pm 0.09$ M$_\odot$. Cubic interpolation of the $q - r_1$ data from the ULTRACAM eclipse modelling (see Table 4) yields a scaled WD radius $R_1/a = 0.0078 \pm 0.0004$ for a mass ratio $q = 0.54$, which translates into a WD radius $R_1 = 0.0103 \pm 0.0007$ R$_\odot$. The WD surface gravity derived from the measured mass and radius is $\log g = 8.36$, in good agreement with the $\log g \simeq 8.35$ value found from spectral modelling (Section 5.1). When the WD radius is used in the WD spectral modelling a distance of ~763 pc is derived, which is consistent with the results presented in Section 6.2 (see Table 6).

Circular polarimetry observations of SW Sex stars show that some systems may contain magnetic WDs (Rodríguez-Gil et al. 2001, 2002; Rodríguez-Gil, Martínez-Pais & de la Cruz Rodríguez 2009). In order to check for any Zeeman splitting in the WD spectrum of HS 0220+0603, we compare the average H β absorption profile of HS 0220+0603 with three magnetic WDs (Fig. 8): SDSS J151130.17+422023.00 ($T_{\rm eff} = 30\,882$ K, $B_1 = 8.4$ MG; Kepler et al. 2013), SDSS J154305.67+343223.6 ($T_{\rm eff} = 25\,000$ K, $B_1 = 4.1$ MG; Külebi et al. 2009) and SDSS J091005.44+081512.2 ($T_{\rm eff} = 25\,000$ K, $B_1 = 1.0$ MG; Külebi et al. 2009). We can therefore rule out a WD magnetic field in excess of 8 MG in HS 0220+0603, but $B_1 \lesssim 4.1$ MG would pass undetected due to the poor signal-to-noise ratio. Blue spectra of better quality are needed to confirm any Zeeman splitting in the low state.

Observations of accreting WDs in CVs indicate that they are significantly more massive than isolated WDs. The statistical studies of the CV population by Smith & Dhillon (1998) and Knigge (2006) produced mean WD masses of 0.80 ± 0.22 M$_\odot$ (above the period gap, 0.69 ± 0.13 M$_\odot$ below) and 0.75 ± 0.05 M$_\odot$, respectively. Also, Savoury et al. (2011) and Zorotovic, Schreiber & Gänsicke (2011) report more massive WDs in CVs. The WD mass for HS 0220+0603 fits well within these results. In addition, the WD mass of the eclipsing dwarf nova IP Peg ($P = 3.80$ h) is measured to be 1.16 ± 0.02 M$_\odot$ (Copperwheat et al. 2010). On the other hand, the mass distribution of isolated WDs peaks at $\lesssim 0.6$ M$_\odot$ (e.g. Koester, Schulz & Weidemann 1979; Bergeron, Saffer & Liebert 1992; Kepler et al. 2007; Falcon et al. 2010; Tremblay et al. 2013).

The distribution of WD effective temperature as a function of the orbital period may serve as a probe of CV evolution. Changes in the mass transfer rate reflect in the WD effective temperature, which is determined by compressional heating of the WD by the accreted matter. Therefore, $T_{\rm eff}$ can be a good tracer of the medium-term (10^3–10^5 yr) mass transfer rate (Townsley & Bildsten 2003; Townsley & Gänsicke 2009). The WD effective temperatures predicted by the evolutionary sequences of Knigge et al. (2011) are significantly cooler than the data below the period gap, and show large disagreement in the 3–4 h orbital period range, where the scarce measurements point to much hotter WDs than expected (see fig. 5 of Townsley & Gänsicke 2009 and fig. 16 of Knigge et al. 2011). However, the relationship between the time-averaged mass transfer rate and the WD temperature has to be used with caution. As Townsley & Gänsicke (2009) point out, the mass transfer rate for a given $T_{\rm eff}$ strongly depends on the WD mass, which again highlights the need for independent mass measurements. In addition, a dominant WD in the blue/UV is also a requirement for a reliable $T_{\rm eff}$ determination. Hence, studies of the WDs in CVs in the low state like the one presented here are important to test the current CV evolutionary sequences in the 3–4 h regime. In this regard, Knigge et al. (2011) suggest that the large scatter of the WD temperatures observed in this orbital period interval may be the result of the temperatures not tracing the secular mass transfer rates.

The measured temperature and mass of the WD in HS 0220+0603 result in a time-averaged mass transfer rate of $\langle \dot{M} \rangle = (1.1 \pm 1.2) \times 10^{-9}$ M$_\odot$ yr^{-1}. This value places HS 0220+0603 closer to the evolutionary sequences of Knigge et al. (2011) than MV Lyr, TT Ari and DW UMa, but at the same time increases the scatter in $\dot{M}$ observed close to the upper edge of the period gap (fig. 5 of Townsley & Gänsicke 2009). In contrast, IP Peg (also in the 3–4 h orbital period regime) may have a time-averaged mass transfer rate as low as $\langle \dot{M} \rangle < 5 \times 10^{-11}$ M$_\odot$ yr^{-1} as derived from its WD temperature (10 000–15 000 K; Copperwheat et al. 2010), almost 30 times lesser than the value inferred for HS 0220+0603 from its WD temperature. These authors also point out the possibility that the WD temperature might not be a good tracer of the medium-term mass transfer rate. The time-averaged mass transfer rate of IP Peg is also inconsistent with the results of the population synthesis study by Howell et al. (2001). It is therefore clear that more direct measurements of masses and temperatures of WDs in the 3–4 h orbital period regime are needed.

7.2 The M-type companion

We have shown that HS 0220+0603 contains an M-dwarf donor star with mass $M_2 = 0.47 \pm 0.05$ M$_\odot$ (Table 6). Note that the

Downloaded from https://academic.oup.com/mnras/article-abstract/452/1/146/1748480/Dynamical-masses-of-a-nova-like-variable-on-the
by University of Sheffield user
on 17 October 2017

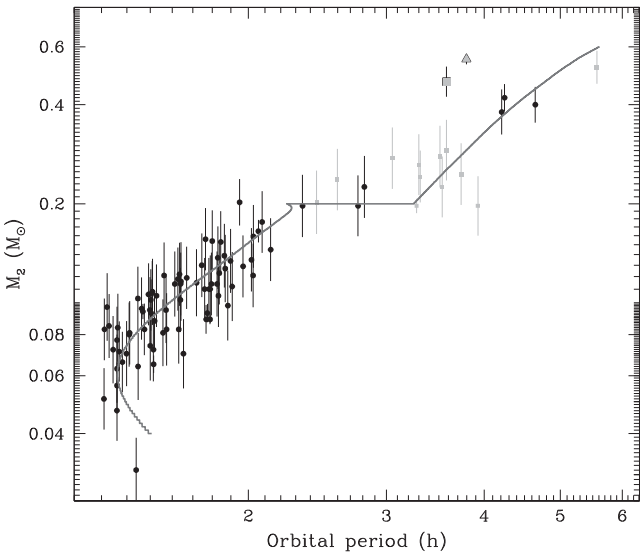

Figure 9. Period–mass data of CV donors (data from Knigge 2006). All mass estimates come from superhump period excesses. The SW Sex systems are marked with grey squares. The large grey square corresponds to our results for HS 0220+0603 while IP Peg is plotted as a large grey triangle. The dark grey solid line shows the best-fitting evolutionary model track of Knigge et al. (2011).

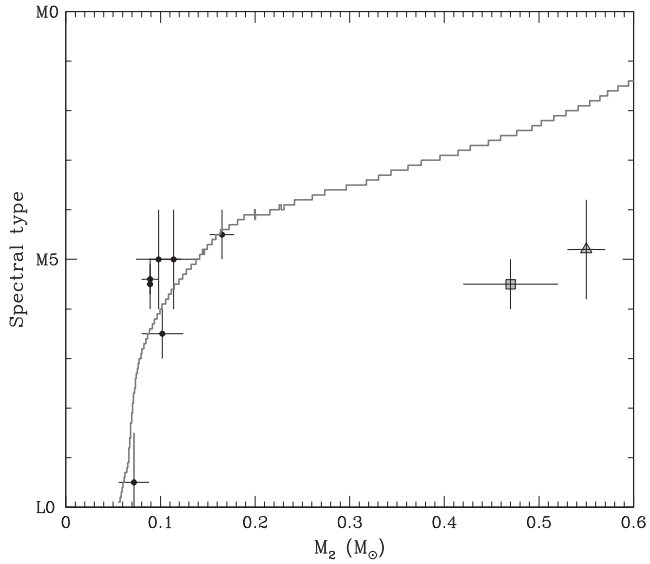

Figure 10. Same as Fig. 9 but for the donor mass–spectral type data. HS 0220+0603 and IP Peg largely deviate from the evolutionary track of Knigge et al. (2011).

fits presented in Section 6.2 never produced a secondary star mass smaller than 0.3 $M_\odot$. We have approximated the radius of the donor star by its Roche lobe volume radius (Eggleton 1983). The donor radius can then be derived from its scaled value R_2/a by using the binary parameters of HS 0220+0603. The resulting Roche lobe volume radius of the M-dwarf is then $R_2 = 0.43 \pm 0.03$ $R_\odot$. The distance to the system when this radius is taken into account in the M-dwarf spectral modelling is found to range between 740 and 940 pc for the spectral types M5 and M6, respectively. This is consistent with both the distances from the WD spectral modelling and the dynamical modelling presented in Section 6.2.

However, our derived mass for the secondary star runs counter to expectations for an orbital period of 3.58 h. The semi-empirical CV evolution track of Knigge et al. (2011) points to an M-dwarf mass of 0.25 $M_\odot$. In Fig. 9, we show the P–M_2 diagram for CVs along with the evolutionary track of Knigge et al. (2011). Note that all mass values are not direct measurements but come from superhump period excesses, as emphasized in Section 1. The SW Sex systems between 3 and 4 h have been plotted as grey filled squares. We have also plotted the data for the dwarf nova IP Peg (large grey triangle), with an orbital period of 3.80 h and a secondary star mass of 0.55 ± 0.02 $M_\odot$. The secondary star in IP Peg is significantly more massive than predicted by the evolutionary track of Knigge et al. (2011). In addition, the measured mass of the secondary star in HS 0220+0603 marginally fits in the predicted orbital period–secondary mass distribution for CVs of Howell et al. (2001, cf. their fig. 5), while the secondary mass in IP Peg is clearly off.

With measured values of 0.55 $M_\odot$ and 0.47 $R_\odot$, Copperwheat et al. (2010) conclude that the secondary star in IP Peg is undersized for its mass, suggesting it is in thermal equilibrium. The same might be happening in HS 0220+0603 with a secondary star mass of 0.47 $M_\odot$ and a derived secondary Roche lobe volume radius of 0.43 $R_\odot$. Taken at face value, this indicates that the donor star in HS 0220+0603 may not be bloated at all. This is not common among CVs, in which the secondary stars are believed to be significantly oversized for their mass as the result of either nuclear evolution or being out of thermal equilibrium.

In Fig. 10, we have plotted the (few) CVs with determinations of both the secondary star mass and spectral type. HS 0220+0603 is marked by a large grey square and IP Peg is plotted with a large grey triangle. Our analysis provided a secondary star spectral type of M5.5 ± 0.5 when the donor star is observed at its inferior conjunction (i.e. phase zero). This indicates a photosphere with temperature around 2800 K (see e.g. Bonnefoy et al. 2014, and references therein). Even if HS 0220+0603 followed the semi-empirical sequence of Knigge et al. (2011) and had a donor mass of 0.25 $M_\odot$, the spectral type would still be cooler than expected. Fig. 10 also shows that the secondary star in IP Peg is underluminous for its mass. The spectral types measured for HS 0220+0603 and IP Peg are also much later than predicted (Howell et al. 2001, cf. the effective temperature–orbital period distribution for CVs in their fig. 7). Again, we stress the fact that we measured the M5.5 ± 0.5 spectral type of the secondary star in HS 0220+0603 from the average of spectra taken at orbital phases around its inferior conjunction, so any information on spectral type change along the orbit is lost. An illustrative example is the case of the polar CV ST LMi, whose secondary star shows a changing temperature with a much cooler region at orbital phase 0.8 (Howell et al. 2000). Therefore, more detailed studies of the secondary stars in the NL variables which populate the 3–4 h orbital period range during low states should be conducted in order to check how frequent these secondary stars are.

8 CONCLUSIONS

We have presented the first dynamical characterization of an eclipsing SW Sex star in the 3–4 h orbital period range during a low state (see Table 7).

We obtained time-resolved optical spectroscopy and photometry of HS 0220+0603 during its 2004–2005 low state. We refined the eclipse ephemeris by including new mid-eclipse times form the photometry. Spectral modelling of the secondary star spectra taken around primary eclipse revealed a spectral type of M5.5 ± 0.5,

Downloaded from https://academic.oup.com/mnras/article-abstract/452/1/146/1748480/Dynamical-masses-of-a-nova-like-variable-on-the
by University of Sheffield user
on 17 October 2017

Table 7. System parameters for HS 0220+0603. R_2 is the volume radius of the secondary star's Roche lobe as defined by Eggleton (1983).

Parameter	Value
q	0.54 ± 0.03
a ($R_\odot$)	1.31 ± 0.03
M_1 ($M_\odot$)	0.87 ± 0.09
R_1 ($R_\odot$)	0.0103 ± 0.0007
T_1 (K)	30 000 ± 5 000
M_2 ($M_\odot$)	0.47 ± 0.05
R_2 ($R_\odot$)	0.43 ± 0.03
K_2 (km s^{-1})	284 ± 11
i (°)	∼79
d (pc)	740 ± 26

suggesting an effective temperature of about 2800 K. The analysis of the spectrum of HS 0220+0603 also provided the first detection of a DAB WD in a CV, with $T_{\rm eff} = 30\,000 \pm 5000$ K. By modelling the ULTRACAM light curve of the WD eclipse, we determined solutions in the binary mass ratio–inclination angle plane. Furthermore, by simultaneously fitting the radial velocity and irradiated ellipsoidal light curves of the secondary star, we independently calculate solutions as well as the unperturbed radial velocity amplitude of the secondary star ($K_2 = 284 \pm 11$ km s^{-1}) and the distance to the source ($d = 740 \pm 26$ pc). Combining the results of the WD and secondary-star modelling we derived the stellar masses to be $M_1 = 0.87 \pm 0.09$ $M_\odot$ and $M_2 = 0.47 \pm 0.05$ $M_\odot$ for the WD and M dwarf, respectively. As in IP Peg, the M-dwarf in HS 0220+0603 seems too cool and undersized for its mass. More binary parameters from dynamical measurements in NL CVs with orbital periods between 3 and 4 h during low states are needed before a critical comparison with theoretical predictions can be made. What triggers low states in CVs is still far from being fully understood.

ACKNOWLEDGEMENTS

We thank Christian Knigge and Mercedes López-Morales for enlightening discussion. We are also thankful to the anonymous referee for the helpful comments and constructive suggestions for improvement of the manuscript. The use of the MOLLY package developed by Tom Marsh is acknowledged. This research has been supported by the Spanish Ministry of Economy and Competitiveness (MINECO) under the grants AYA2012–38700 and AYA2010–18080. PRG acknowledges support from the MINECO under the Ramón y Cajal programme (RYC–2010–05762). He also acknowledges support from the XMM grant NNG05GJ22G. He is thankful to the staff of the Harvard–Smithsonian Centre for Astrophysics for a pleasant visit during which part of this work was carried out. He also wishes to thank all the M1 Group observers for their long-term dedication to the search for low states. TRM and DS acknowledge support from the UK's Science and Technology Facilities Council, grant ST/L000733/1. The research leading to these results has received funding from the European Research Council under the European Union's Seventh Framework Programme FP 2007–2013 ERC Grant Agreement no. 320964 (WDTracer). MRS acknowledges support from FONDECYT (grant 1141269) and from the Millennium Nucleus RC130007 (Chilean Ministry of Economy). VSD and ULTRACAM are supported by the STFC. Based in part on observations collected at the European Organization for Astronomical Research in the Southern hemisphere, Chile, under programme 074.D–0657, and on observations obtained with *XMM–Newton*, an ESA science mission with instruments and contributions directly funded by ESA Member States and NASA, and on observations made with the WHT operated on the island of La Palma by the Isaac Newton Group in the Spanish Observatorio del Roque de los Muchachos, and on observations made with the NOT operated by the Nordic Optical Telescope Scientific Association at the Observatorio del Roque de los Muchachos, La Palma, Spain, and on observations made with the IAC80 telescope operated on the island of Tenerife by the Instituto de Astrofísica de Canarias in the Spanish Observatorio del Teide. The WHT data were obtained as part of the 2004 International Time Programme of the night-time telescopes at the European Northern Observatory.

REFERENCES

Araujo-Betancor S., Gänsicke B. T., Long K. S., Beuermann K., de Martino D., Sion E. M., Szkody P., 2005, ApJ, 622, 589
Arnaud K. A., 1996, in Jacoby G. H., Barnes J., eds, ASP Conf. Ser. Vol. 101, Astronomical Data Analysis Software and Systems V. Astron. Soc. Pac., San Francisco, p. 17
Bergeron P., Saffer R. A., Liebert J., 1992, ApJ, 394, 228
Bianchini A., 1992, in Vogt N., ed., ASP Conf. Ser. Vol. 29, Vina del Mar Workshop on Cataclysmic Variable Stars. Astron. Soc. Pac., San Francisco, p. 284
Billington I., Marsh T. R., Dhillon V. S., 1996, MNRAS, 278, 673
Boeshaar P. C., 1976, PhD thesis, Ohio State Univ.
Bonnefoy M., Chauvin G., Lagrange A.-M., Rojo P., Allard F., Pinte C., Dumas C., Homeier D., 2014, A&A, 562, A127
Chabrier G., Baraffe I., 1997, A&A, 327, 1039
Ciardi D. R., Howell S. B., Hauschildt P. H., Allard F., 1998, ApJ, 504, 450
Claret A., 1998, A&A, 335, 647
Cook B. A., Williams P. K. G., Berger E., 2014, ApJ, 785, 10
Copperwheat C. M., Marsh T. R., Dhillon V. S., Littlefair S. P., Hickman R., Gänsicke B. T., Southworth J., 2010, MNRAS, 402, 1824
Cox J. P., Giuli R. T. eds 1969, Principles of Stellar Structure, Vol. II. Gordon & Breach, New York
de Jong J. A., van Paradijs J., Augusteijn T., 1996, A&A, 314, 484
Dhillon V. S., Jones D. H. P., Marsh T. R., 1994, MNRAS, 266, 859
Dhillon V. S. et al., 2007, MNRAS, 378, 825
Eggleton P. P., 1983, ApJ, 268, 368
Falcon R. E., Winget D. E., Montgomery M. H., Williams K. A., 2010, ApJ, 712, 585
Gabriel M., 1969, in Kumar S. S., ed., Low-Luminosity Stars. Gordon & Breach, New York, p. 267
Gänsicke B. T. et al., 2009, MNRAS, 397, 2170
Gianninas A., Strickland B. D., Kilic M., Bergeron P., 2013, ApJ, 766, 3
Gupta A., Galeazzi M., Williams B., 2011, ApJ, 731, 63
Güver T., Özel F., 2009, MNRAS, 400, 2050
Hauschildt P. H., Allard F., Baron E., 1999, ApJ, 512, 377
Hessman F. V., Gänsicke B. T., Mattei J. A., 2000, A&A, 361, 952
Horne K., 1986, PASP, 98, 609
Howell S. B., Ciardi D. R., Dhillon V. S., Skidmore W., 2000, ApJ, 530, 904
Howell S. B., Nelson L. A., Rappaport S., 2001, ApJ, 550, 897
Jansen F. et al., 2001, A&A, 365, L1
Kafka S., Ribeiro T., Baptista R., Honeycutt R. K., Robertson J. W., 2008, ApJ, 688, 1302
Kalberla P. M. W., Burton W. B., Hartmann D., Arnal E. M., Bajaja E., Morras R., Pöppel W. G. L., 2005, MNRAS, 440, 775
Kepler S. O., Kleinman S. J., Nitta A., Koester D., Castanheira B. G., Giovannini O., Costa A. F. M., Althaus L., 2007, MNRAS, 375, 1315
Kepler S. O. et al., 2013, MNRAS, 429, 2934
King A. R., Cannizzo J. K., 1998, ApJ, 499, 348
Kirkpatrick J. D., Henry T. J., McCarthy D. W., 1991, ApJS, 77, 417
Kleinman S. J. et al., 2004, ApJ, 607, 426

Downloaded from https://academic.oup.com/mnras/article-abstract/452/1/146/1748480/Dynamical-masses-of-a-nova-like-variable-on-the
by University of Sheffield user
on 17 October 2017

Knigge C., 2006, MNRAS, 373, 484
Knigge C., Baraffe I., Patterson J., 2011, ApJS, 194, 28
Koester D., Schulz H., Weidemann V., 1979, A&A, 76, 262
Külebi B., Jordan S., Euchner F., Gänsicke B. T., Hirsch H., 2009, A&A, 506, 1341
Leggett S. K., Allard F., Berriman G., Dahn C. C., Hauschildt P. H., 1996, ApJS, 104, 117
Lépine S., Rich R. M., Shara M. M., 2003, AJ, 125, 1598
Livio M., Pringle J. E., 1994, ApJ, 427, 956
Lucy L. B., 1967, Z. Astrophys., 65, 89
Manser C. J., Gänsicke B. T., 2014, MNRAS, 442, L23
Mason K. O. et al., 2001, A&A, 365, L36
Mason E., Howell S. B., Barman T., Szkody P., Wickramasinghe D., 2008, A&A, 490, 279
Patterson J. et al., 2005, PASP, 117, 1204
Phillips S. N., Shahbaz T., Podsiadlowski P., 1999, MNRAS, 304, 839
Pizzolato N., Maggio A., Micela G., Sciortino S., Ventura P., 2003, A&A, 397, 147
Pyrzas S. et al., 2009, MNRAS, 394, 978
Reid I. N., Hawley S. L., Gizis J. E., 1995, AJ, 110, 1838
Reiners A., Mohanty S., 2012, ApJ, 746, 43
Rodríguez-Gil P., Casares J., Martínez-Pais I. G., Hakala P., Steeghs D., 2001, ApJ, 548, L49
Rodríguez-Gil P., Casares J., Martínez-Pais I. G., Hakala P. J., 2002, in ASP Conf. Ser. Vol. 261, The Physics of Cataclysmic Variables and Related Objects. Astron. Soc. Pac., San Francisco, p. 533
Rodríguez-Gil P. et al., 2007, MNRAS, 377, 1747
Rodríguez-Gil P., Martínez-Pais I. G., de La Cruz Rodríguez J., 2009, MNRAS, 395, 973
Rodríguez-Gil P., Schmidtobreick L., Long K. S., Gänsicke B. T., Torres M. A. P., Rubio-Díez M. M., Santander-García M., 2012, MNRAS, 422, 2332
Savoury C. D. J. et al., 2011, MNRAS, 415, 2025
Schlafly E. F., Finkbeiner D. P., 2011, ApJ, 737, 103
Schmidtobreick L., Rodríguez-Gil P., Long K. S., Gänsicke B. T., Tappert C., Torres M. A. P., 2012, MNRAS, 422, 731
Schmitt J. H. M. M., Liefke C., 2004, A&A, 417, 651
Schreiber M. R., Gänsicke B. T., Mattei J. A., 2002, A&A, 384, L6
Schreiber M. R. et al., 2010, A&A, 513, L7
Shahbaz T., Groot P., Phillips S. N., Casares J., Charles P. A., van Paradijs J., 2000, MNRAS, 314, 747
Shahbaz T., Zurita C., Casares J., Dubus G., Charles P. A., Wagner R. M., Ryan E., 2003, ApJ, 585, 443
Shahbaz T., Casares J., Watson C. A., Charles P. A., Hynes R. I., Shih S. C., Steeghs D., 2004, ApJ, 616, L123
Smith D. A., Dhillon V. S., 1998, MNRAS, 301, 767
Smith R. K., Brickhouse N. S., Liedahl D. A., Raymond J. C., 2001, ApJ, 556, L91
Strüder L. et al., 2001, A&A, 365, L18
Thorstensen J. R., Ringwald F. A., Wade R. A., Schmidt G. D., Norsworthy J. E., 1991, AJ, 102, 272
Townsley D. M., Bildsten L., 2003, ApJ, 596, L227
Townsley D. M., Gänsicke B. T., 2009, ApJ, 693, 1007
Tremblay P.-E., Ludwig H.-G., Steffen M., Freytag B., 2013, A&A, 559, A104
Tsang B. T. H., Pun C. S. J., Di Stefano R., Li K. L., Kong A. K. H., 2012, ApJ, 754, 107
Turner M. J. L. et al., 2001, A&A, 365, L27
Wade R. A., Horne K., 1988, ApJ, 324, 411
Zorotovic M., Schreiber M. R., Gänsicke B. T., 2011, A&A, 536, A42

This paper has been typeset from a TEX/LATEX file prepared by the author.

Downloaded from https://academic.oup.com/mnras/article-abstract/452/1/146/1748480/Dynamical-masses-of-a-nova-like-variable-on-the
by University of Sheffield user
on 17 October 2017